

June 2007

# Optimization of carbon nanotube synthesis from porous anodic Al–Fe–Al templates

Matthew Maschmann

*Purdue University, [maschmann@purdue.edu](mailto:maschmann@purdue.edu)*

Aaron D. Franklin

*Birck Nanotechnology Center and School of Electrical and Computer Engineering, Purdue University, [aaron-franklin@purdue.edu](mailto:aaron-franklin@purdue.edu)*

Timothy D. Sands

*Birck Nanotechnology Center and Purdue University, [tsands@purdue.edu](mailto:tsands@purdue.edu)*

Timothy Fisher

*Birck Nanotechnology Center and Purdue University, [tsfisher@purdue.edu](mailto:tsfisher@purdue.edu)*

Follow this and additional works at: <http://docs.lib.purdue.edu/nanopub>

---

Maschmann, Matthew; Franklin, Aaron D.; Sands, Timothy D.; and Fisher, Timothy, "Optimization of carbon nanotube synthesis from porous anodic Al–Fe–Al templates" (2007). *Birck and NCN Publications*. Paper 67.  
<http://docs.lib.purdue.edu/nanopub/67>

This document has been made available through Purdue e-Pubs, a service of the Purdue University Libraries. Please contact [epubs@purdue.edu](mailto:epubs@purdue.edu) for additional information.

# Optimization of carbon nanotube synthesis from porous anodic Al–Fe–Al templates

Matthew R. Maschmann<sup>a,b</sup>, Aaron D. Franklin<sup>a,c</sup>, Timothy D. Sands<sup>a,c,d</sup>,  
Timothy S. Fisher<sup>a,b,\*</sup>

<sup>a</sup> Birk Nanotechnology Center, Purdue University, West Lafayette, IN 47907, United States

<sup>b</sup> School of Mechanical Engineering, Purdue University, West Lafayette, IN 47907, United States

<sup>c</sup> School of Electrical and Computer Engineering, Purdue University, West Lafayette, IN 47907, United States

<sup>d</sup> School of Materials Engineering, Purdue University, West Lafayette, IN 47907, United States

Received 3 November 2006; accepted 30 May 2007

Available online 28 June 2007

## Abstract

A parametric study of carbon nanotube (CNT) synthesis from catalytically active porous anodic Al–Fe–Al multilayer templates was conducted with respect to pore aspect ratio, Fe layer thickness, CNT synthesis temperature, and pre-anodization thermal annealing. Performance metrics included CNT catalytic activity and the pore wall integrity at the Al–Fe–Al interface. The observed CNT density was a strong function of pore diameter, synthesis temperature and pre-anodization annealing of the catalyst film. Vertical pore wall integrity at the Al–Fe–Al interface was optimized by selection of pre-anodization annealing conditions, with interfacial void formation observed in the absence of this technique. Based on CNT growth rates, an activation energy of 0.52 eV was observed for CNT synthesis for all film structures, regardless of pore aspect ratio. The optimization of templated CNT synthesis is expected to assist in the development of high-density vertically oriented CNT-based devices.

© 2007 Elsevier Ltd. All rights reserved.

## 1. Introduction

Single-walled CNTs (SWNTs) and double-walled CNTs (DWNTs) have been incorporated into a myriad of devices such as electronics [1,2], sensors [3,4], and electron emitters [5,6] because of their excellent transport and mechanical properties [7]. However, one major impediment to the realization of functional and scalable CNT-based devices is achieving synthesis of individual CNTs that may be readily functionalized at predefined locations on a substrate. Recently we have reported the synthesis of a silicon-supported porous anodic Al–Fe–Al film structure that facilitates the selective catalytic growth of SWNTs and DWNTs [8], as confirmed by HRTEM and micro-Raman

spectroscopy. The structure allows for straightforward fabrication of electrical contacts [9] by electrodeposition of metal nanowires [10], leading to the establishment of CNT devices embedded in the template's vertical pores. For high-density CNT device integration, uninterrupted vertical pore order (without branching) and a large population of pores containing CNTs are required to produce one functional device per vertical pore. A detailed parameter study of the porous anodic Al–Fe–Al multilayer structure with respect to CNT synthesis and pore wall integrity, however, has not previously been reported and would assist in the production of high-density CNT devices.

The anodization of thin Al foils and supported Al films to form porous anodic alumina (PAA) has been rigorously studied and is relatively well understood. PAA films have been used for templated growth of metallic nanowires [10–12] and for the synthesis of large-diameter multi-walled CNTs (MWNTs) [13–17]. In addition, the anodization of co-sputtered films of Al and Fe (with uniformly distributed

\* Corresponding author. Address: Birk Nanotechnology Center, Purdue University, West Lafayette, IN 47907, United States. Fax: +1 765 494 0539.

E-mail address: [tsfisher@purdue.edu](mailto:tsfisher@purdue.edu) (T.S. Fisher).

Fe) has been studied with Fe concentrations of 4at.% [18] and 7.5at.% [19] using 0.01 M ammonium pentaborate as an anodization electrolyte. When anodized above threshold potentials, these nonporous anodized films developed voids due to the encapsulation of oxygen gas produced during the incorporation of Fe into the anodized film. The threshold voltages for void formation depended on Fe concentration in the alloy and decreased from a value of 300 V at 4at.% Fe to 100 V for 7.5at.% Fe. Anodization of the alloy below the threshold value resulted in a uniform anodic film having a Fe concentration similar to that of the beginning metal alloy. The anodization of a thin film stack composed of a localized thin Fe film incorporated between two Al layers, however, has not been analyzed. This work characterizes these types of anodized film in terms of structural stability and their ability to promote the catalytic production of CNTs.

CNT synthesis from catalytically active porous anodic Al–Fe–Al multilayer templates was examined with respect to pore aspect ratio, which is related to the pore diameter and top alumina thickness, Fe layer thickness, CNT synthesis temperature, and pre-anodization thermal annealing of the film. Characterization of synthesis products is based on the CNT density after PECVD processing and vertical pore wall integrity at the Al–Fe–Al interface. In addition, average CNT growth rates are quantified as a function of synthesis temperature, allowing for the determination of the CNT synthesis activation energy using the templated catalyst.

## 2. Experimental

Synthesis of the catalytic film structures analyzed in this study began by successive deposition of  $\text{SiO}_x$ , Ti, Al, Fe, and Al on a thermally oxidized Si wafer using electron beam evaporation at a base pressure of  $5 \times 10^{-7}$  Torr or less. For all samples, bottom layers consisting of 50 nm  $\text{SiO}_x$ , 150 nm Ti, and 100 nm Al were utilized. The  $\text{SiO}_x$  layer acted as an adhesion layer between the substrate and metal film stack, while the Ti layer may be used as an electrode for further processing, such as electrodeposition of metallic nanowires [10]. The bottom Al layer thickness was chosen based on optimum conditions for Pd deposition on CNTs from other experiments [8] and had no effect on CNT synthesis. Fe catalyst layer thicknesses ranged from 0.5 to 20 nm. Deposition rates of all metals other than Fe were maintained at 1 nm/s or less, while the deposition of Fe was maintained at approximately 0.1 nm/s or less. An illustration of a typical film stack appears in Fig. 1.

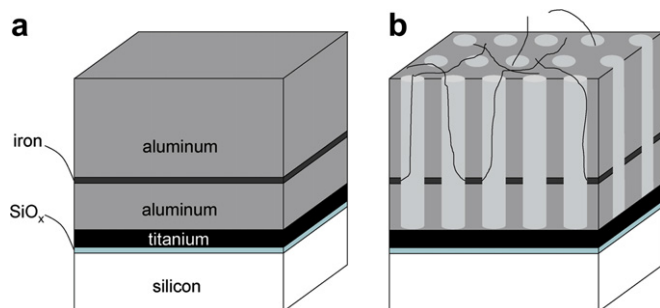


Fig. 1. Schematic of porous anodic Al–Fe–Al catalyst film (a) prior to anodization and (b) after anodization and CNT synthesis.

Anodization of the Al and Fe layers proceeded using standard two-step anodization procedures [20]. The anodization electrolytes employed include 0.3 M oxalic acid and 0.3 M sulfuric acid maintained at 5 °C. Anodization voltages included 40 V for templates anodized using oxalic acid, and 20 V for templates anodized using sulfuric acid. Pore diameter and pitch were controlled by the anodization electrolyte and voltage [21]. The height of the top anodized alumina layer was controlled by thickness of the top Al deposition and the duration of the first anodization step, followed by subsequent removal using the two-step procedure. The anodization current for Al layers was approximately 10 mA/cm<sup>2</sup>, while the current reached as high as 1 A/cm<sup>2</sup> during anodization of the embedded Fe layer, depending on the Fe layer thickness and pre-anodization thermal annealing conditions, discussed in subsequent sections. The current produced during anodization of the Fe layer for samples that had undergone thermal annealing was always significantly less than that of a similar sample not undergoing the annealing step and was similar to that observed for pure aluminum.

The pore diameter, height of the top alumina layer, and aspect ratio, defined as the height of the top alumina layer surface divided by average pore diameter, were examined to determine their influence on CNT catalysis. Although the precise transport mechanism of hydrocarbons to the catalyst layer is unknown, the pore diameter and depth of the embedded Fe layer are expected to play important roles in the availability of reactive hydrocarbons for CNT catalysis. Anodized films consisting of three separate pore configurations were examined. All films contained common bottom layers of 50 nm  $\text{SiO}_x$ , 150 nm Ti, and 200 nm Al. Films anodized with sulfuric acid employed a 350 nm top alumina layer and displayed an average pore diameter of approximately 15 nm. Films anodized with oxalic acid included a top alumina layer thickness of 350 or 700 nm and displayed an average pore diameter of approximately 30 nm. The resulting aspect ratio of the films anodized using sulfuric acid was 24, while those anodized using oxalic acid were 12 and 24 for top alumina layer thicknesses of 350 and 700 nm, respectively. These pore geometries were chosen because they allow for a decoupling of the effects of pore length, diameter, and aspect ratio.

CNTs synthesis occurred in a microwave plasma-enhanced chemical vapor deposition (PECVD) system. Synthesis conditions were chosen based on optimized conditions used for SWNT growth using a MgO supported Mo/Co catalyst structure [22] and previous experience with the catalyst structure [8]. Standard synthesis conditions included 10 Torr pressure, 10 sccm  $\text{CH}_4$ , 50 sccm  $\text{H}_2$ , and 300 W plasma. Synthesis temperature was varied from 650 to 900 °C. The synthesis began upon introduction of  $\text{CH}_4$  gas once the sample reached the synthesis temperature. Upon completion of synthesis, microwave plasma power and substrate heating were immediately turned off, and chamber gases were evacuated. The application of a negative dc bias, which has been shown to enhance vertical alignment of SWNTs in this system, was not incorporated in this study, as it has been associated with a decrease in SWNT density [23].

After synthesis, samples were imaged using a Hitachi S-4800 field-emission scanning electron microscope (FESEM). CNT length was measured on the anodized structure's top surface using a field of view angled 15° from the cross-section, while pore wall integrity was observed by cleaving a sample and imaging the cross-section.

## 3. Results and discussion

### 3.1. Effect of pore aspect ratio

The pore aspect ratio, defined as the quotient of the top alumina layer thickness and average pore diameter, is expected to regulate the transport of hydrocarbon precursors to the Fe catalyst layer. To determine the influence of pore aspect ratio on CNT synthesis, the CNT spatial density and length were observed using FESEM for each template. Figure 2a and b displays typical CNT densities

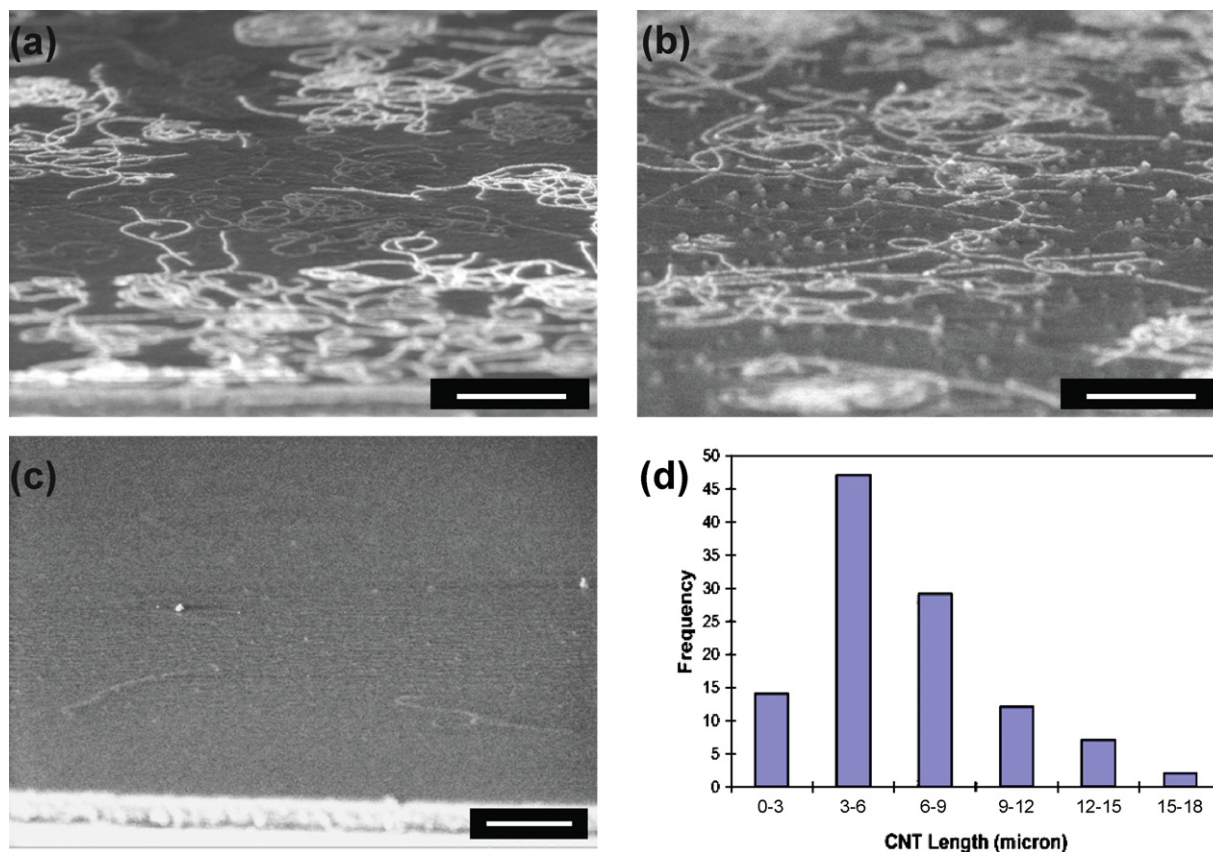


Fig. 2. CNT growth at 850 °C for 3 min using porous anodic Al–Fe–Al structures. Tilted FESEM micrographs of CNTs on templates consisting of (a) 350 nm, (b) 700 nm top alumina layer anodized using oxalic acid, (c) 350 nm top alumina layer anodized using sulfuric acid and (d) histogram of CNT length for the sample with a 700 nm top alumina layer anodized using oxalic acid. Scale bars = 2 microns.

observed for templates anodized in oxalic acid. CNT density decreased slightly as the height of the top alumina layer increased from 350 nm (Fig. 2a) to 700 nm (Fig. 2b), consistent with growth of large-diameter CNTs from PAA templates [24]. Although templates anodized using sulfuric acid exhibit a greater density of pores per area than those anodized using oxalic acid, use of templates anodized with sulfuric acid resulted in a significantly lower CNT density (Fig. 2c). The dramatic decrease in CNT density associated with the template anodized in sulfuric acid compared to a film of similar aspect ratio (i.e. 24) anodized in oxalic acid suggests that pore diameter may have a more direct effect on CNT density than the aspect ratio or depth of the embedded Fe layer. Therefore, the cross-sectional area of the pore openings is an important factor in allowing access of hydrocarbon molecules to the catalyst layer.

To quantify the CNT growth from the templates previously mentioned, average CNT growth rates as functions of synthesis temperature were determined. After PECVD synthesis, CNTs were examined by angled cross-sectional FESEM to determine their length distributions on the top PAA surface, as described above. CNTs chosen for measurement appeared to be isolated, not associated with bundles of multiple CNTs. CNT lengths were calculated by tracing the CNT paths on the top alumina surface using

graphical software and comparing the pixel count value of the CNT to that of the scale bar length, taking into account the tilt angle of the alumina surface. The depth of the top alumina layer was then added to the CNT length measured on the top surface to compute a total CNT length. A sample size of 75 or greater CNTs was obtained from no fewer than five micrographs for each temperature, with a typical histogram of CNT lengths shown in Fig. 2d. Because the density of CNTs synthesized from templates anodized in oxalic acid above 850 °C was too large to distinguish individual CNT lengths, CNTs synthesized from templates anodized in sulfuric acid were used to assess products grown at high temperatures due to their lower CNT density. Conversely, the density of CNTs synthesized from templates anodized in sulfuric acid was too sparse below 800 °C to obtain a significant sample size, and CNTs synthesized from templates anodized in oxalic acid were employed for this synthesis temperature regime. We also note that electron charging effects between the CNTs and the top alumina surface produced high-contrast FESEM features of CNTs on the top film surface, and greatly exaggerated the apparent CNT diameters [8].

Although the average growth rate of the CNTs decreased with total synthesis time, as also observed by others [25,26], the difference between average growth rates

at different synthesis temperatures remains approximately constant for synthesis times greater than 1 min, as shown in Fig. 3a. Consequently, the activation energy calculated from the average growth rate for these syntheses is relatively insensitive to the chosen synthesis time of 3 min. Also of importance, CNT density increases significantly for synthesis times greater than 1 min, allowing for a more significant sample size in calculating the average growth rate. Considering these points, it is safe to assume that the average observed CNT growth rate for processes longer than 1 min accurately captures the average CNT length for the sample. A time of 3 min was chosen as a basis for comparison for all samples, as this time yielded CNTs with lengths that could be more easily imaged by FESEM. This synthesis time is also thought to be sufficiently long to minimize the effects of potential non-homogeneous conditions at the beginning and end of each growth process. Average growth rates of CNTs from the three film configurations as a function of synthesis temperature are shown in the Arrhenius plot in Fig. 3b. Error bars indicate the 95% confidence interval of the average CNT growth rate. Although CNT density varies between film structures, Fig. 3b shows that the average growth rate for a given temperature is statistically equivalent for all template aspect ratios at the common synthesis temperature of 850 °C.

Applying an exponential line fit to the combined data in Fig. 3b, the average growth rate can be related to the rate of carbon diffusion into catalyst particles. The relationship is assumed to follow an Arrhenius form given as

$$k = Ae^{-E_{\text{act}}/RT}$$

where  $k$  is the rate of carbon diffusion,  $A$  is a pre-exponential factor,  $E_{\text{act}}$  is the synthesis activation energy,  $R$  is the universal gas constant, and  $T$  is absolute synthesis temperature. Based on the Arrhenius law and the data in Fig. 3b, an activation energy of  $53 \pm 9$  kJ/mol, or  $0.52 \pm 0.08$  eV, is derived with a 95% confidence level for CNTs grown from the templated structures. Typical reported activation ener-

gies observed for PECVD synthesis of MWNTs using  $\text{C}_2\text{H}_2$  as a carbon source are 0.30 eV with a Fe catalyst [27] and range from 0.23 to 0.76 eV for a Ni catalyst employing  $\text{CH}_4$  as a carbon source [27–31]. For comparison, activation energies of 1.21 [27] and 1.23 eV [32] have been reported for similar synthesis conditions using thermal CVD with Ni and Fe catalyst, respectively.

### 3.2. Effect of Fe catalyst thickness

The thickness of the initial Fe layer influences the amount of catalytically active material available in the cell walls for CNT synthesis. However, during anodization of the Fe-rich interfacial region, material around the circumference of a pore is compressed by excessive oxygen formation [18,19], causing inter-pore void formations and necking of the interfacial region, as seen in Fig. 5a. The anodization at and around the abrupt Fe-rich layer leads to a sudden loss of anodization equilibrium and results in a re-initiation of pore spacing as anodization continues past the Al–Fe–Al interface in the bottom Al layer. Consequently, vertical pore walls are often interrupted at the Al–Fe–Al interfacial region, resulting in a high percentage of branching pores rather than purely vertical pores from the top PAA surface to the Ti layer.

During CNT synthesis, much of the catalytically active Fe-rich alumina is likely to be located in the necked region between pores, out of the direct line of sight of incoming hydrocarbons. As a result, catalyst activity may be hindered by interfacial void formation. Although an increase in the Fe layer's thickness increases total Fe content, an increased Fe concentration correlates to increased void formation. In addition, anodization of samples with an initial Fe layer thickness of 5 nm or greater often produced sufficient damage to the template to delaminate the film at the Al–Fe–Al interface during anodization. Very little correlation between Fe layer thickness and CNT density is observed for Fe layers between 1 and 20 nm, although

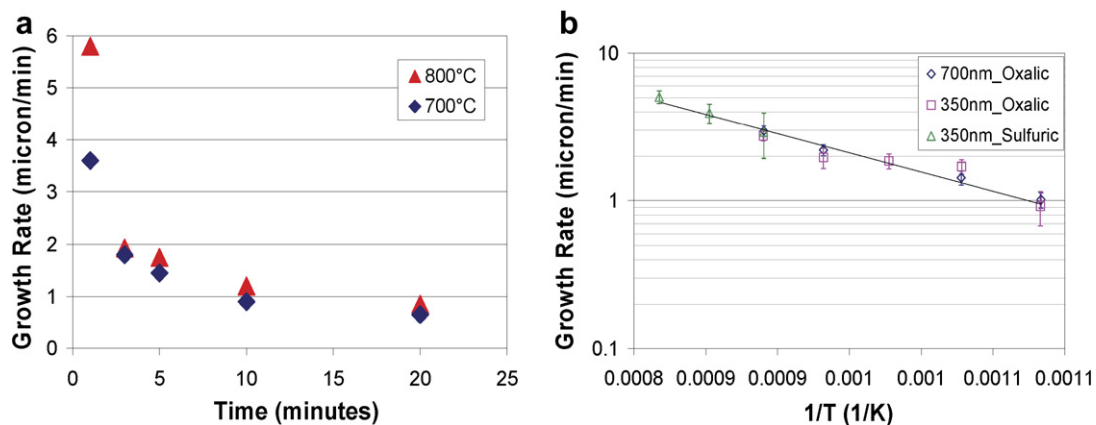


Fig. 3. CNT growth rate for porous anodic Al–Fe–Al structures. (a) Average growth rate for sample with 350 nm top alumina layer and anodized in oxalic acid with CNT synthesis temperatures of 700 and 800 °C. (b) Arrhenius plot for average CNT growth rates.

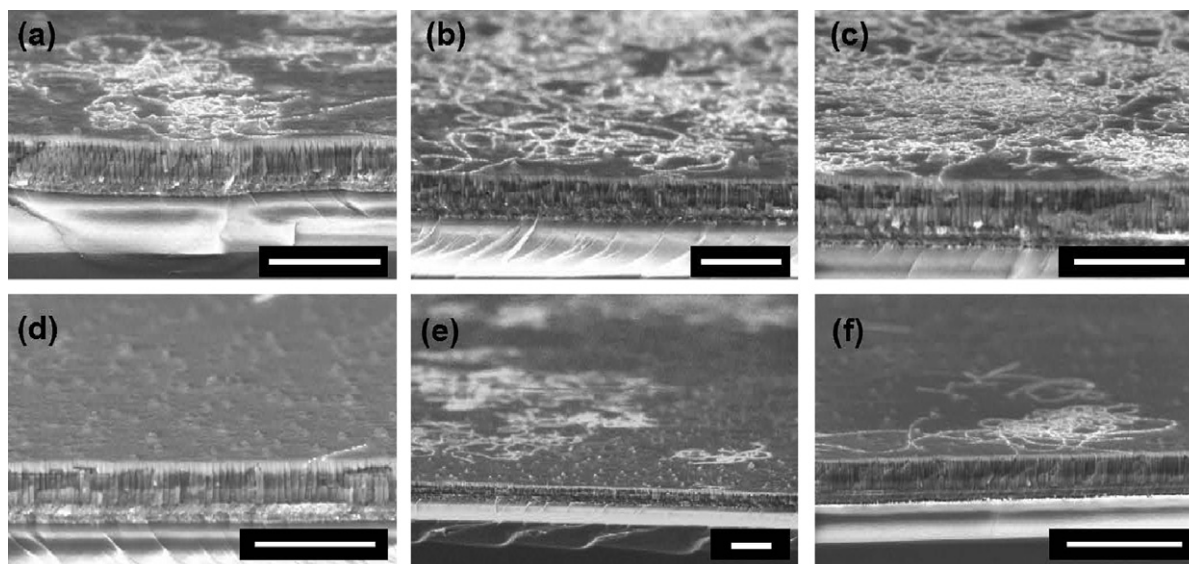


Fig. 4. Comparison of CNT density for various Fe layer thicknesses. Titled cross-sectional FESEM micrographs of samples having undergone pre-anodization 500 °C annealing for 20 min incorporating (a) 0.5 nm, (b) 1.0 nm, and (c) 2.0 nm Fe layers. Tilted cross-sectional FESEM micrographs of samples without pre-anodization annealing with samples incorporating (d) 0.5 nm, (e) 1.0 nm, and (f) 2.0 nm Fe layers. Scale bars = 1 micron.

decreased density is observed for a 0.5 nm Fe layer thickness or less, as shown in Fig. 4d–f.

### 3.3. Effect of pre-anodization annealing

To diffuse Fe into the surrounding Al films and reduce the Fe concentration at the interface, thermal annealing of the film stack was performed prior to anodization. Process temperatures from 300 to 550 °C in a dry air ambient were studied with various Al–Fe–Al film configurations. An annealing temperature above 550 °C severely affected the planarity of the anodized film surface, while temperatures of 400 °C or less were insufficient to affect the morphology of the anodized structure for durations less than several hours. The temperature range between 450 and 500 °C was studied in greater detail, as it produced planar films and noticeable changes in the anodized template.

The deposited Fe layer thickness plays a significant role in the effectiveness of the annealing process in terms of the

resulting CNT density. A thicker initial Fe layer produces a larger total Fe dose and a higher Fe concentration throughout the effective diffusion length for a given annealing temperature and time. Because of the thin Fe layer relative to the Al layers on either side, intermetallic FeAl<sub>3</sub> islands are likely formed at the annealing temperature studied herein. Anodization may then proceed between FeAl<sub>3</sub> islands, resulting in relatively smooth vertical pore walls and islands of Fe-rich material directly available to incoming hydrocarbon gasses. As a result, pre-anodization annealing increases the catalytically active area and produces vertical pores that are not interrupted at the Al–Fe–Al interface.

Fig. 4 shows the effect of pre-anodization annealing and Fe layer thickness on resulting CNT density. Fe catalyst thicknesses were varied from 0.5 to 2 nm, while annealing was performed at 500 °C for 20 min. Annealed samples exhibit a dramatic increase in CNT density compared to samples with similar Fe thicknesses that were not annealed.

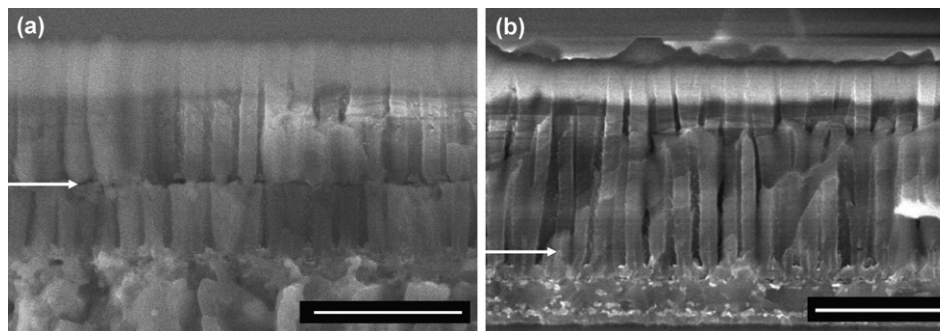


Fig. 5. Cross-sectional FESEM micrograph of templates using a 0.5 nm Fe layer (a) without pre-anodization annealing and (b) with 20 min pre-anodization annealing at 450 °C. Arrows denote the location of the deposited Fe layer. Scale bars = 500 nm.

In addition, an increase in CNT density is observed with increasing Fe thickness when annealing is employed, while only sporadic growth is observed on samples that were not annealed.

Vertical pore wall integrity is greatly improved with pre-anodization annealing as well. Fig. 5 shows the effect of thermal annealing at 450 °C for 20 min using a template containing a 0.5 nm Fe layer, an annealing condition that produced optimal pore wall integrity. It is clear that inter-pore necking at the Fe layer is nearly removed, resulting in smooth vertical pore walls. Vertical pores (without branching) are important for incorporating CNTs grown from the template into functional devices, ensuring that one device exists per pore [9].

#### 4. Conclusions

A parametric study investigating the effects of pore aspect ratio, Fe layer thickness, synthesis temperature and thermal annealing of catalytically active porous anodic Al–Fe–Al templates with respect to catalytic activity and pore wall integrity has been conducted. The study reveals that CNT catalytic activity increases substantially with increased pore diameter and pre-anodization annealing and only slightly with increased top alumina layer thickness. An activation energy of 0.52 eV was derived by leveraging CNT growth rates from various template film configurations. Proper choice of thermal annealing conditions greatly enhanced CNT density and assisted in the formation of vertical pore walls, free of voids, during anodization. The results of this study are expected to extend the functionality of CNTs synthesized from anodized Al–Fe–Al structures.

#### Acknowledgements

The authors gratefully acknowledge funding from the NASA-Purdue Institute for Nanoelectronics and Computing and the Birck Nanotechnology Center in support of this work.

#### References

- [1] Javey A, Guo J, Wang Q, Lundstrom M, Dai H. Ballistic carbon nanotube field effect transistors. *Nature* 2003;424:654–7.
- [2] Shimada T, Sugai T, Ohno Y, Kishimoto S, Mizutani T, Yoshida H, et al. Double-wall carbon nanotube field-effect transistors: ambipolar transport characteristics. *Appl Phys Lett* 2004;84:2412–4.
- [3] Mu S-C, Tang H-L, Qian S-H, Pan M, Yuan R-Z. Hydrogen storage in carbon nanotubes modified by microwave plasma etching and Pd decoration. *Carbon* 2006;44:762–7.
- [4] Kim B-K, Park N, Na PS, So H-M, Kim J-J, Kim H, et al. The effect of metal cluster coatings on carbon nanotubes. *Nanotechnology* 2006;17:496–500.
- [5] Bonard J-M, Salvétat J-P, Stockli T, de Heer WA, Forro L, Chatelain A. Field emission from single-wall carbon nanotube films. *Appl Phys Lett* 1998;73:918–20.
- [6] Son YW, Oh S, Ihm J, Han S. Field emission properties of double-wall carbon nanotubes. *Nanotechnology* 2005;16:125–8.
- [7] Li Y, Wang K, Wei J, Gu Z, Wang Z, Lauo J, et al. Tensile properties of long aligned double-walled carbon nanotubes. *Carbon* 2005;43:31–5.
- [8] Maschmann MR, Franklin AD, Amama PB, Zakharov DN, Stach EA, Sands TD, et al. Vertical single- and double-walled carbon nanotubes grown from modified porous anodic alumina templates. *Nanotechnology* 2006;17:3925–9.
- [9] Maschmann MR, Franklin AD, Scott A, Janes DB, Sands TD, Fisher TS. Lithography-free in situ ohmic contacts to single-walled carbon nanotubes. *Nano Lett* 2006;6:2712–7.
- [10] Franklin AD, Maschmann MR, DaSilva M, Janes DB, Fisher TS, Sands TD. In-place fabrication of nanowire electrode arrays for vertical nanoelectronics on Si substrates. *J Vac Sci B* 2007;25:343–7.
- [11] Rabin O, Herz PR, Lin Y-M, Akinwande AI, Cronin SB, Dresselhaus MS. Formation of thick porous anodic alumina films and nanowire arrays on silicon wafers and glass. *Adv Func Mat* 2003;13:631–8.
- [12] Tian M, Xu S, Wang J, Kumar N, Wertz E, Li Q, et al. Penetrating the oxide barrier in situ and separating freestanding porous anodic alumina films in one step. *Nano Lett* 2005;5:697–703.
- [13] Che G, Lakshmi BB, Martin CR, Fisher ER. Chemical vapor deposition based on synthesis of carbon nanotubes and nanofibers using a template method. *Chem Mater* 1998;10:260–7.
- [14] Li J, Papadopoulos C, Xu JM. Highly ordered carbon nanotube arrays for electronics applications. *Appl Phys Lett* 1999;75:367–9.
- [15] Suh JS, Lee JS. Highly ordered two-dimensional carbon nanotube arrays. *Appl Phys Lett* 1999;75:2047–9.
- [16] Jeong S-H, Hwang HY, Hwang S-K, Lee K-H. Carbon nanotubes based on anodic aluminum oxide nano-template. *Carbon* 2004;42:2073–80.
- [17] Yen J-H, Leu I-C, Wu M-T, Lin C-C, Hon M-H. Density control of carbon nanotube arrays synthesized by ICP-CVD using AAO/Si as a nanotemplate. *Electrochem Solid State* 2004;7:H29–31.
- [18] Habazaki H, Takahiro K, Yamaguchi S, Shimizu K, Skeldon P, Thompson GE, et al. Development of iron-rich layers during anodic oxidation of sputter-deposited Al-4 atom% Fe alloy. *J Electrochem Soc* 1999;146:2502–7.
- [19] Habazaki H, Shimizu K, Skeldon P, Thompson GE, Wood G. The behaviour of iron during anodic oxidation of sputter-deposited Al–Fe alloys. *Corros Sci* 2001;43:1393–402.
- [20] Masuda H, Satoh M. Fabrication of gold nanodot array using anodic porous alumina as an evaporation mask. *Jpn J Appl Phys* 1996;35:L126–9.
- [21] Li AP, Muller F, Birner A, Nielsch K, Gosele U. Hexagonal pore arrays with a 50–420 nm interpore distance formed by self-organization in anodic alumina. *J Appl Phys* 1998;84:6023–6.
- [22] Maschmann MR, Amama PB, Goyal A, Iqbal Z, Gat R, Fisher TS. Parametric study of synthesis conditions in plasma-enhanced CVD of high-quality single-walled carbon nanotubes. *Carbon* 2006;44:10–8.
- [23] Maschmann MR, Amama PB, Goyal A, Iqbal Z, Fisher TS. Freestanding vertically oriented single-walled carbon nanotubes synthesized using microwave plasma-enhanced CVD. *Carbon* 2006;44:2758–63.
- [24] Yen J-H, Leu I-C, Wu M-T, Lin C-C, Hon M-H. Density control for carbon nanotube arrays synthesized by ICP-CVD using AAO/Si as a nanotemplate. *Electrochem Solid State* 2004;7:H29–31.
- [25] Yang H-S, Kang H-D, Min B-K, Lee H-R. Dynamic growth rate behaviour of a carbon nanotube forest characterized by in situ optical growth rate. *Nano Lett* 2003;3:863–5.
- [26] Sharma R, Rez P, Treacy MMJ, Stuart SJ. In situ observation of the growth mechanisms of carbon nanotubes under diverse reaction conditions. *J Electron Microsc* 2005;54:231–7.
- [27] Hofman S, Csanyi G, Ferrari AC, Payne MC, Robertson J. Surface diffusion: the low activation energy path for nanotube growth. *Phys Rev Lett* 2005;95:036101–4.
- [28] Boskovic BO, Stolojan V, Khan RUA, Haq S, Silva RP. Large-area synthesis of carbon nanofibres at room temperature. *Nature Mat* 2002;1:165–8.

- [29] Ducati C, Alexandrou I, Chhowalla M, Amaratunga GAJ, Robertson J. Temperature selective growth of carbon nanotubes by chemical vapor deposition. *J Appl Phys* 2002;92:3299–303.
- [30] Yang C-J, Chen Chih. Characterization and field-emission properties of carbon nanotube arrays in nanoporous alumina template and on blank Si substrate. *J Appl Phys* 2006;100:104302-1–6.
- [31] Hofman S, Ducati C, Robertson J, Kleinsorge B. Low-temperature growth of carbon nanotubes by plasma-enhanced chemical vapor deposition. *Appl Phys Lett* 2003;83:135–7.
- [32] Lee YT, Park J, Choi YS, Ryu H, Lee HJ. Temperature-dependent growth of vertically aligned carbon nanotubes in the range 800–1100 °C. *J Phys Chem B* 2002;106:7614–8.